Mechanisms of dark decay of holograms in lithium niobate crystals

Yunping Yang
Department of Electrical Engineering, California Institute of Technology, Pasadena, CA 91125
yunping@sunoptics.caltech.edu

Ingo Nee, Karsten Buse
Universität Bonn, Physikalisches Institut, Wegelerstraβe 8, D-53115 Bonn, Germany
inee, kbuse@uni-bonn.de

Demetri Psaltis
Department of Electrical Engineering, California Institute of Technology, Pasadena, CA 91125
psaltis@sunoptics.caltech.edu

Abstract: The lifetimes of non-fixed holograms in $LiNbO_3$ crystals with different dopants, doping levels and oxidation states have been measured in the temperature range from 30 to 180° C. Two dark decay mechanisms have been identified: proton compensation and electron tunneling. For $LiNbO_3$ crystals with low doping levels, the dominant mechanism of dark decay is proton compensation with the activation energy of 1.0 eV. This mechanism is independent of dopant, doping level and oxidation state. For $LiNbO_3$ with high doping levels, the prevailing mechanism is electron tunneling with the activation energy much less than that of proton compensation, e.g., 0.28 eV for $LiNbO_3$:0.25 wt% Fe_2O_3. The dark decay of holograms stored in crystals with medium doping levels is the result of a combination of both effects.
OCIS codes: (090.2900) Holographic recording materials; (090.7330) Volume holographic gratings; (210.0210) Optical data storage; (160.3730) Lithium niobate

Introduction

Photorefractive $LiNbO_3$ crystals have been of intense interest in the fields of holographic data storage [1] and narrow-band wavelength filters for optical telecommunications [2-4]. Photorefractive volume phase gratings can be produced in electro-optic materials by redistribution of excited carriers in the presence of light. One of the most important issues is the dark decay due to the dark conductivity. The time constant of the dark decay τ is defined as the time until the grating strength decays in the dark to $1/e$ of the original value and is related to the dark conductivity σ_d as $\tau = \varepsilon_0\varepsilon/\sigma_d$, where ε is the dielectric constant of lithium niobate. Lifetimes of non-fixed holograms in $LiNbO_3$ crystals vary between a few minutes and one year [5-7]. These lifetimes are generally too short for practical applications. In order to improve the lifetimes, a good understanding of the origins of the dark decay is needed.

Recently it has been found that in the dark and at room temperature electron tunneling between iron sites occurs in highly-doped $LiNbO_3$:Fe crystals [7]. It is generally accepted that for the temperature range between 150 and 200° C the proton conductivity is enlarged by several orders of magnitude compared to that at room temperature. This behavior is used for thermal fixing [8]. For temperatures higher than 200° C, excitation of electrons into the conduction band is supposed to be the main process

OSA TOPS Vol. 62 Photorefractive Effects, Materials, and Devices
D. Nolte, G. Salamo, A. Siahmakoun, and S. Stepanov, eds.

[9]. Up to now the thermal activation energy of the electron tunneling process is unknown. A study of the process at and close to room temperature is of special importance. Lifetime estimates of holograms stored in lithium niobate are frequently based on extrapolation of high temperature data. This is risky because proper thermal activation energies must be used. In this work, the dark decay of holographic gratings in $LiNbO_3$ crystals with different dopants, doping levels and oxidation states in the temperature range from 30 to 180° C has been measured. From the experimental data, two different activation energies have been extracted, namely, 1.0 eV and 0.28 eV. These two activation energies are identified to correspond to different dark decay mechanisms: proton compensation and electron tunneling [7], respectively.

Materials and method

Congruently melting $LiNbO_3$ samples are used. Table 1 summarizes some parameters of these samples. All these crystals were x-cut and polished to optical quality. Thermal annealing in various atmospheres is used to achieve desired oxidation states and proton concentrations. For all $LiNbO_3$:Fe crystals used, the shape of the absorption spectra is the same, i.e., we avoid too strong reduction that generates, e.g., polaron and bipolaron bands. Thus the Fe^{2+} concentration c_{Fe2+} can be calculated from absorption measurements. Because iron occurs only in the valence states 2+ and 3+, the concentration of Fe^{3+} is determined by subtracting c_{Fe2+} from the entire iron concentration c_{Fe}. For $LiNbO_3$:Mn crystals, the oxidation states are difficult to determine quantitatively since their absorption spectrum are very broad and there is no apparent characteristic absorption peak for Mn center. The absorption coefficient at the maximum of the OH^- absorption at 2870 nm is used to calculate the proton concentration [10].

Table 1. Summary of parameters of the samples

Sample	Doping level	Oxidation state	Notes
S1, LN:Fe	0.05 wt% Fe_2O_3	$c_{Fe2+}/c_{Fe3+} = 0.05$	Proton-enriched
S2, LN:Fe	0.05 wt% Fe_2O_3	$c_{Fe2+}/c_{Fe3+} = 0.21$	Proton-reduced
S3, LN:Mn	0.02 wt% MnO	Medium	As grown
S4, LN:Mn	0.1 wt% MnO	Reduced	Proton-reduced
S5, LN:Mn	0.1 wt% MnO	Oxidized	Proton-reduced
S6, LN:Fe	0.25 wt% Fe_2O_3	$c_{Fe2+}/c_{Fe3+} = 0.10$	Proton-reduced
S7, LN:Fe	0.138 wt% Fe_2O_3		As grown
S8, LN:Fe	0.138 wt% Fe_2O_3	$c_{Fe2+}/c_{Fe3+} = 0.03$	Proton-enriched
S9, LN:Fe	0.138 wt% Fe_2O_3	$c_{Fe2+}/c_{Fe3+} = 0.03$	Proton-reduced

The crystals were placed on a heatable plate that was temperature-controlled within 0.1° C accuracy. An argon-ion laser beam with the wavelength 514 nm was used in all of the experiments to record holograms. The laser beam was split into two extraordinarily polarized beams of equal intensity, that were expanded to cover the whole crystal during recording. All recorded holograms had a grating period of 1.3 μm and were written with the grating vector oriented along the c-axis. Recording was always performed at room temperature. Afterwards, the crystals were heated to a certain temperature in the dark and a weak laser beam of 514 nm was used to monitor the holographic diffraction efficiency. The weak readout light illuminated the crystal only from time to time, and the intervals between two measurements were long enough to keep the erasure of the holograms by the probing beam negligible.

After each experiment the crystal was heated to 230° C and kept at this temperature under uniform illumination for about 45 minutes to erase the gratings completely.

Proton compensation

The two crystals with the doping level 0.05 wt% Fe_2O_3, S1 and S2, were cut from the same boule. Sample S1 was proton-enriched by suitable annealing treatment while sample S2 was proton-reduced. The proton concentrations of sample S1 and sample S2 were 5.5×10^{18} cm^{-3} and 3.1×10^{17} cm^{-3}, respectively. Figure 1 shows the measured dark decay time constants of these two crystals. The time constants of both crystals obey an Arrhenius-type dependence on the absolute temperature T, $\tau = \tau_0 \exp(E_a/k_BT)$, where τ_0 is a pre-exponential factor, k_B is the Boltzmann constant, and E_a is the activation energy. There are several justifications that the dark decay in these two crystals is dominated by proton compensation of the electrical space-charge field. The activation energies obtained for the samples S1 and S2 are almost the same, 0.97 eV and 1.0 eV, respectively, and close to the proton activation energies reported in the literature [8, 11]. The ratio of the fitted pre-exponential factors for the samples S2 and S1 is 18.3, which is, as it should be, almost equal to the reciprocal ratio of the proton concentrations of these two samples, namely, 17.7. Noting the fact that sample S2 is reduced much more than sample S1 but the pre-exponential factor of sample S1 is even less than that of sample S2, we can rule out the possibility that the dark decay is related to the iron-doping and electronic band transport since the time constant of the dark decay due to band transport should be inversely proportional to the oxidation state c_{Fe2+}/ c_{Fe3+}. We would like to emphasize the large range of temperatures used. Measurements were taken from room temperature up to 180° C.

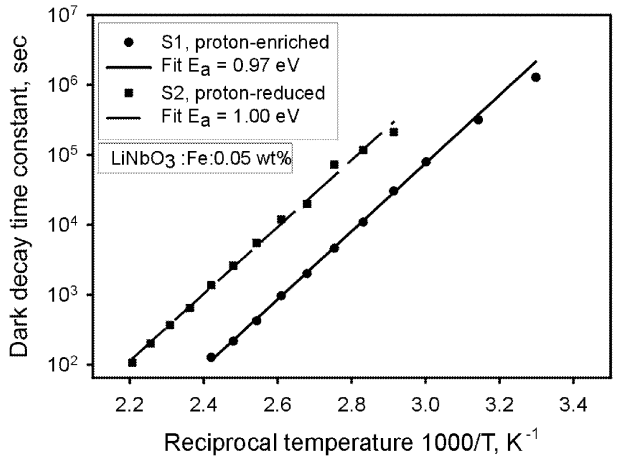

Fig. 1. Arrhenius plot of the dark decay time constants of holograms stored in $LiNbO_3$:Fe crystals with a doping level of 0.05 wt% Fe_2O_3, sample S1: proton-enriched, sample S2: proton-reduced.

Figure 2 shows the measured dark decay time constants of three $LiNbO_3$:Mn crystals S3, S4 and S5. Again, the time constants of these crystals obey an Arrhenius-type dependence on the absolute temperature with almost the same activation energy 1.00 eV, which is equal to that of sample S1 and S2. The fitted pre-exponential factors of S3, S4 and S5 are inversely proportional to their proton concentrations. We also measured the lifetimes of non-fixed holograms stored in $LiNbO_3$:Ce crystals with the doping level of 0.02 wt% Ce_2O_3. The experimental results of dark decay for the $LiNbO_3$:Ce crystals have shown the same behaviors as those of samples S1-S5, and the dark decay in all these $LiNbO_3$ crystals is due to proton compensation to the space charge field.

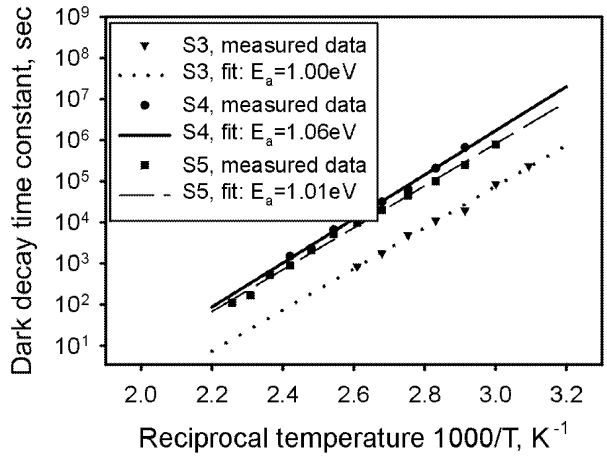

Fig. 2. Arrhenius plot of the dark decay time constants of holograms stored in $LiNbO_3$:Mn crystals, sample S3: 0.02 wt% MnO, as grown; sample S4: 0.1 wt% MnO, proton-reduced; sample S5: 0.1wt% MnO, proton-reduced.

Electron tunneling

Figure 3 shows the measured dark decay time constants for sample S6, a $LiNbO_3$:Fe crystal doped with 0.25 wt% Fe_2O_3. Although the plot is still Arrhenius-like, the activation energy, 0.28 eV, is much smaller than that of samples S1 and S2. Obviously, there is a mechanism other than proton compensation dominating the dark decay. This mechanism has been identified as electron tunneling between sites of Fe^{2+} and Fe^{3+} [7]. It is interesting that just increasing the doping level by a factor of 5 yields a totally different dark decay mechanism. This type of dark decay limits the highest practical doping level for $LiNbO_3$:Fe crystals.

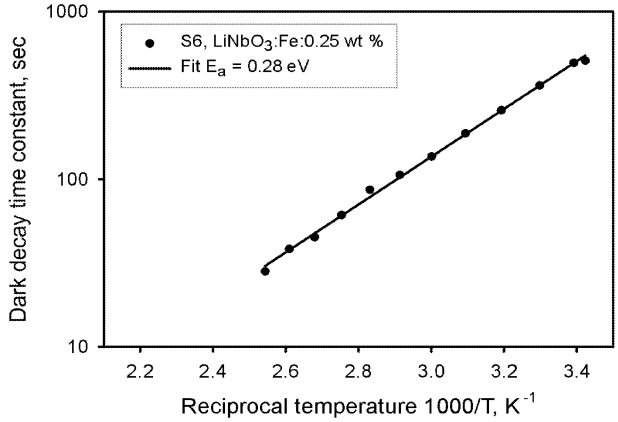

Fig. 3. Arrhenius plot of dark decay time constants of holograms in $LiNbO_3$:Fe crystals with a doping level of 0.25 wt% Fe_2O_3, sample S6: proton-reduced.

One important characteristic of electron tunneling between dopant sites is that the probability of tunneling, thus the dark conductivity due to electron tunneling, depends on the effective trap density, N_{eff}, which is defined as $N_{eff} = c_{Fe2+}c_{Fe3+}/(c_{Fe2+}+c_{Fe3+})$ in $LiNbO_3$:Fe crystals. Upon strong thermal reduction (much more Fe^{2+} than Fe^{3+} present), a lack of empty sites diminishes the dark conductivity. The dark conductivity due to electron tunneling is supposed to be roughly proportional to the effective trap density. Figure 4 shows exactly what we expect. The dark decay time constants of sample S7, a $LiNbO_3$:0.138 wt% Fe_2O_3 crystal, with different oxidation states at room temperature have been

measured. The dark conductivities σ_d were calculated as $\sigma_d = \varepsilon_0\varepsilon/\tau$ and plotted versus effective trap density N_{eff} in Figure 4.

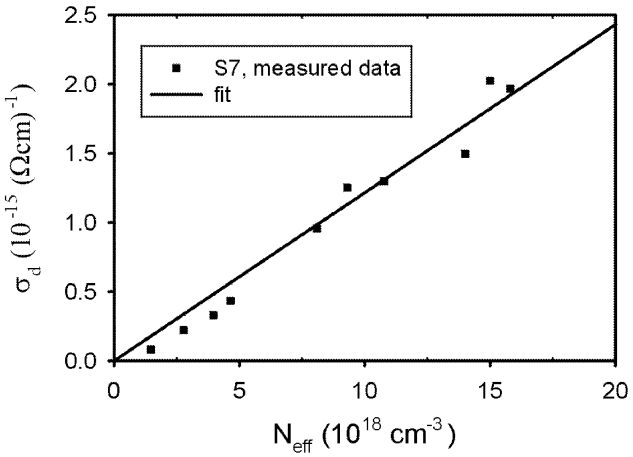

Fig. 4. Dark conductivities σ_d vs effective trap density N_{eff} in sample S7, a $LiNbO_3$:0.138 wt% Fe_2O_3 crystal [7].

Another important characteristic of electron tunneling is that the probability of tunneling is an exponential function of the mean distance between dopant sites. In $LiNbO_3$:Fe crystals, the mean distance between two closest Fe sites can be approximately calculated as $(c_{Fe})^{1/3}$, where c_{Fe} is the entire Fe concentration. Considering the effective trap density, the dark conductivity due to electron tunneling σ_d should be proportional to $N_{eff}\times\exp[\alpha\ (c_{Fe})^{1/3}]$, where α is a constant. Figure 5 shows a semilogarithmic plot of the normalized dark conductivity due to electron tunneling, $(\sigma_d-\sigma_{d,0})/\ N_{eff}$, versus the third root of the iron concentration, where $\sigma_{d,0}$ is the iron-independent background conductivity. The experimental data are well described by an exponential growth of the normalized dark conductivity with $(c_{Fe})^{1/3}$.

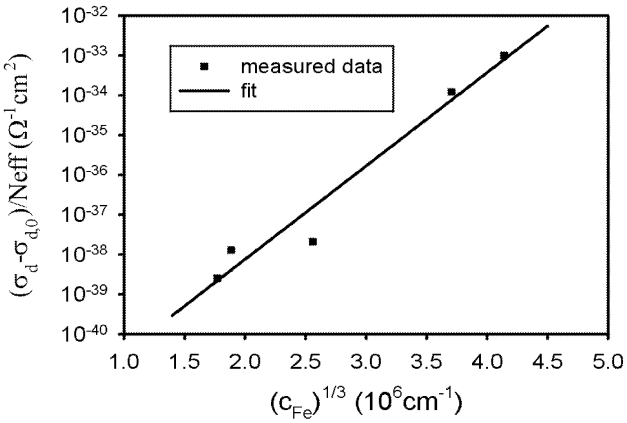

Fig. 5. Semilogarithmic plot of the normalized dark conductivity due to electron tunneling, $(\sigma_d-\sigma_{d,0})/\ N_{eff}$, versus the third root of the iron concentration c_{Fe} [7].

Combination of proton compensation and electron tunneling

For $LiNbO_3$ crystals with low doping levels, proton compensation dominates the dark decay, while for those with a doping level as high as 0.25 wt% Fe_2O_3 the dominant mechanism is electron tunneling. It is reasonable to expect both these two effects to be present in some crystals with doping levels between

0.05 wt% Fe_2O_3 and 0.25 wt% Fe_2O_3. Figure 6 shows exactly the picture that we expect. Two crystals, S8 and S9, each with a doping level of 0.138 wt% Fe_2O_3, have been used. Both of these crystals were cut from the same boule. Sample S8 was proton-enriched and sample S9 was proton-reduced with proton concentrations 5.6×10^{18} cm^{-3} and 3.0×10^{17} cm^{-3}, respectively. The oxidation states in S8 and S9 are more or less the same.

Since the activation energy of proton compensation is much larger than that of electron tunneling, the dependence of the time constant on the absolute temperature is stronger for proton compensation. At high temperatures, the proton compensation plays a larger role; thus we see the difference between these two crystals in the high temperature range due to the different proton contents. At low temperatures, e.g., room temperature, the effect of electron tunneling prevails. Since the crystals have the same doping level and the same oxidation state, we should not see much disparity of the dark decay between the samples S8 and S9 at low temperatures, which is exactly what Figure 6 shows. Fitting the data in the low temperature range to an Arrhenius law yields an activation energy close to what we obtained from Figure 3, that is 0.28 eV, which means the dominant dark decay mechanism at room temperature in these two crystals is the same as that in crystal S6.

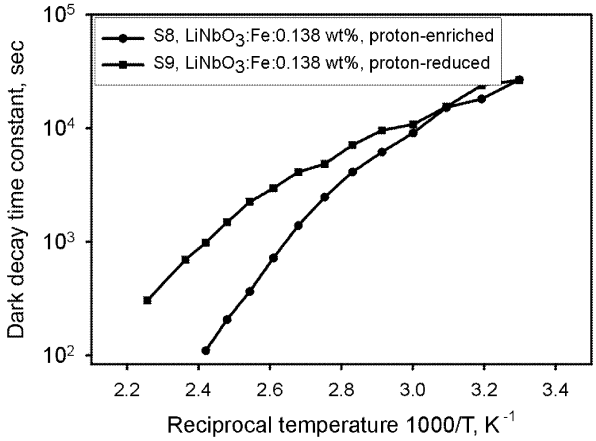

Fig. 6. Dark decay time constant versus reciprocal temperature in $LiNbO_3$:Fe crystals with a doping level of 0.138 wt% Fe_2O_3, sample S8: proton-enriched, sample S9: proton-reduced.

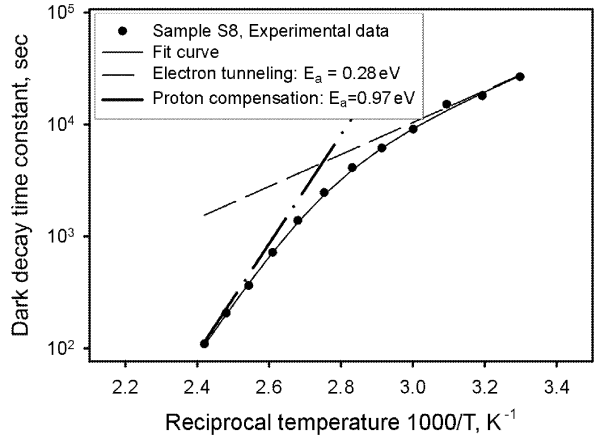

Fig. 7. Dark decay time constant versus reciprocal temperature of sample S8. The solid line is a fit of equation $\tau_d = \tau_p(T)\tau_e(T)/[\tau_d(T)+\tau_d(T)]$ to the experimental data.

In crystals where both, proton compensation and electron tunneling matter, the dark conductivity σ_d should be: $\sigma_d = \sigma_p + \sigma_e$, where σ_p and σ_e are dark conductivity due to proton compensation and electron tunneling, respectively. The decay time constant τ is related to the conductivity σ_d as $\tau = \varepsilon_0\varepsilon/\sigma_d$, so we have $\tau_d=\tau_p(T)\tau_e(T)/[\tau_p(T)+\tau_e(T)]$, where $\tau_p(T)=\tau_{0p}\exp(E_{ap}/k_BT)$ and $\tau_e(T)=\tau_{0e}\exp(E_{ae}/k_BT)$. We fit this equation to the experimental data obtained with sample S8 using a proton compensation activation energy of 0.97 eV and an electron tunneling activation energy of 0.28 eV. The result is shown in Figure 7, which is, as we can see, very good. We also did the fitting with the data obtained with sample S9. From the fitted pre-exponential factors of the proton compensation we estimate that the ratio of the proton concentrations of samples S8 and S9 is about 22, which agrees very well with the factor 19 determined by absorption measurements.

Conclusions

In conclusion, two mechanisms of the dark decay, proton compensation and electron tunneling with activation energies of 1.0 eV and 0.28 eV, respectively, have been identified. In crystals with doping levels less than 0.05 wt% Fe_2O_3, proton compensation dominates the dark decay and extrapolation of lifetimes by an Arrhenius law to room temperature is valid. The time constant of this type of dark decay is inversely proportional to the proton concentration. For crystals with doping levels as high as 0.25 wt% Fe_2O_3, electron tunneling dominates the dark decay. This type of dark decay also limits the highest practical doping level in $LiNbO_3$ crystals in, e.g., holographic storage systems and optical narrow-band wavelength filters. For crystals with medium doping levels e.g., between 0.05 wt% Fe_2O_3 and 0.25 wt% Fe_2O_3, both, proton compensation and electron tunneling, contribute significantly to the dark decay, and the single Arrhenius law does not hold anymore with a single activation energy. Caution is required in extrapolating the lifetime of room temperature holograms from the experimental data obtained at high temperatures.

Acknowledgments

Effort sponsored by NSF, Center for Neuromorphic Systems Engineering ERC, DARPA and Volkswagen-Stiftung. The authors thank the NSF and the DAAD for sponsoring the US-German collaboration.

References

1. H. J. Coufal, D. Psaltis and G. T. Sincerbox, *Holographic Data Storage*, Springer (2000).
2. V. Leyva, G. A. Rakuljic, and B. O'Conner, "Narrow bandwidth volume holographic optical filter operating at the Kr transition at 1547.82 nm," Appl. Phys. Lett. 65, 1079-1081 (1994).
3. R. Müller, M. T. Santos, L. Arizmendi, and J. M. Cabrera, "A narrow-band interference filter with photorefractive $LiNbO_3$," J. Phys. D 27, 241-246 (1994).
4. S. Breer, H. Vogt, I. Nee, and K. Buse, "Low-crosstalk WDM by Bragg diffraction from thermally fixed reflection holograms in lithium niobate," Electron. Lett. 34, 2419-2421 (1998).
5. E. Krätzig and R. Orlowski, "$LiTaO_3$ as Holographic Storage Material," Appl. Phys. 15, 133-139 (1978).
6. D. Kip, J. Hukriede, and E. Krätzig, "Holographic Measurement of Dark Conductivity in $LiNbO_3$:Ti:Fe Planar Optical Waveguides," Phys. Status Solidi A 168, R3-R4 (1998).
7. I. Nee, M. Müller, K. Buse, and E. Krätzig, "Role of iron in lithium-niobate crystals for the dark-storage time of holograms," J. Appl. Phys. 88, 4282-4286 (2000).
8. D. L. Staebler and J. J. Amodei, "Thermally fixed holograms in $LiNbO_3$," Ferroelectrics 3, 107-113 (1972).

9. B. I. Sturman, M. Carrascosa, F. Agullo-Lopez, and J. Limeres, "Theory of high-temperature photorefractive phenomena in $LiNbO_3$ crystals and applications to experiment," Phys. Rev. B : Condens. Matter 57, 12792-12805 (1998).
10. S. Kapphan and A.Breitkopf, "PE-Layers and Proton Diffusion Profiles in $LiNbO_3$ Investigated with Fourier-IR and Second Harmonic Generation," Phys. Status Solidi. A 133, 159-166 (1992).
11. A. Yariv and S. Orlov, "Holographic storage dynamics in lithium niobate: theory and experiment," J. Opt. Soc. Am. B 13, 2513-2523 (1996).